NUMERICAL SENSITIVITY EVALUATION OF THE PHASE-RESOLVING WAVE MODEL SWASH AND ITS APPLICABILITY IN AN OPERATIONAL FORECAST ENVIRONMENT FOR REEF-LINED COASTS

A THESIS SUBMITTED TO THE GRADUATE DIVISION OF THE UNIVERSITY OF HAWAIʻI AT MĀNOA IN PARTIAL FULFILLMENT OF THE REQUIREMENTS FOR THE DEGREE OF

MASTER OF SCIENCE

IN

OCEANOGRAPHY

May 2024

By
Alex Gibbs

Thesis Committee:
Philip Thompson, Ph.D.
Douglas S. Luther, Ph.D.
Justin Stopa, Ph.D.

Dedication

I would like to dedicate this work to my family. Their unwavering support, patience, love, and understanding have been key to my success, providing me with the courage and motivation to pursue my passion for oceanography and research.

I'd also like to dedicate this work to the NOAA's Nearshore Wave Prediction Team, namely, Pablo Santos, Andre Van der Westhuysen, Roberto Padilla, Doug Gaer, and Tony Freeman that I have had the opportunity to be part of over the past 15 years. Their expertise in the field of oceanography and technical abilities within the framework of the National Weather Service has been monumental in shaping the direction that I have taken with research. Their dedication to advancing the field has been a constant source of inspiration through a large portion of my career.

Furthermore, I dedicate this work to the National Weather Service forecast office in Honolulu, HI. Undertaking this research while working as a full-time shift working forecaster, primarily night shifts, was a significant challenge. Routine shift swaps were made with colleagues throughout this endeavor, which in return allowed me to attend classes and make critical deadlines within the academic program.

Acknowledgments

I would like to express my deepest gratitude to my supervisor, Dr. Philip Thompson, for his invaluable guidance, leadership, patience, and mentorship throughout the course of this research. Dr. Thompson's expertise and encouragement have been instrumental in structuring the direction of this thesis.

I am also thankful to the members of my thesis committee, Dr. Douglas Luther and Dr. Justin Stopa, for their insightful feedback and constructive criticism, which have greatly improved my understanding of the work presented in the thesis.

Furthermore, I extend my appreciation to the oceanography administrative office, faculty, and fellow graduate students who have generously shared their time and insights through this experience. Without their support, this research would not have been possible.

Special thanks to Dr. Assaf Azouri for his invaluable tips, data analysis insights, and opinions along the way, which significantly contributed to the techniques used in my analyses.

I am grateful to the University of Hawai'i for providing the resources and facilities necessary for carrying out this work.

Contents

Abstract

An evaluation of the Simulating WAves till SHore (SWASH, *Zijlema et al.* (2011)) spectral wave-flow model on the north shore of Oahu, Hawaii, was conducted to determine sensitivity to various numerical settings and grid configurations. It also aimed to assess what could be achievable in an operational forecasting environment, such as NOAA's National Weather Service Forecast Offices, with regard to computational expenses involved. Spatial resolution, water level, boundary conditions, friction, and the computational time window were analyzed and compared across a two-dimensional (2D) grid and along a one-dimensional transect. Water elevations derived from these tests were evaluated at a nearshore point that remained wet throughout the simulations and used to compare bulk-averaged output parameters that included: sea and swell height (H_{ss}), wave setup (η_s), infragravity wave height (H_{ig}), and the two-percent exceedance wave height ($\eta_{2\%}$). The sensitivity of these bulk quantities to model framework decisions that impact computational expense pose immense challenges for implementation in an operational forecast environment. We present results demonstrating how forecast sites can balance operational feasibility and accuracy.

List of Tables

List of Figures

List of Abbreviations

ADCIRC Advanced Circulation

BEWARE Bayesian Estimator for Wave Attack in Reef Environments

BOSZ Boussinesq Ocean and Surf Zone

BAG Bathymetric Attributed Grid

CFL Courant-Friedrichs-Lewy

CDIP Coastal Data Information Program

CPU Central Processing Unit

CSP Coastal Storm Program

DFT Discrete Fourier Transform

DEM Digital Elevation Model

ENC Electronic Nautical Chart

FSM Federated States of Micronesia

GCD Goddard-Caldwell Database

IG Infragravity

MHHW Mean Higher High Water

MHW Mean High Water

MPI Message Passing Interface

NCEP National Centers for Environmental Prediction

NLSW Nonlinear Shallow Water

NOAA National Oceanic and Atmospheric Administration

NOS National Ocean Service

NWS National Weather Service

NWPS Nearshore Wave Prediction System

NGDC National Geophysical Data Center

PacIOOS Pacific Islands Ocean Observing System

PILOT Pacific Island Land Ocean Typhoon

PS Power Spectrum

PSD Power Spectral Density

RMI Republic of the Marshall Islands

RTOFS Real-Time Ocean Forecast System

SHOALS Scanning Hydrographic Operational Airborne Lidar Survey

SLOSH Sea, Lake, and Overland Surges from Hurricanes

SWAN Simulating Waves Nearshore

SWASH Simulating Waves Til Shore

SWIMS Surge and Wave Island Modeling Studies

USACE United States Army Corps of Engineers

UH-ORE University of Hawai'i Ocean and Resources Engineering

WW3 WAVEWATCH III

XB-SB XBeach - Surfbeat

List of Symbols

γ_{mod} Model Output for a Parameter

γ_{ref} Model Reference for a Parameter

Δf Frequency Bandwidth

$\Delta X/\Delta Y$ Difference in X and Y

$\eta_{2\%}$ 2% Exceedance Height

H_b Breaker Height

H_{ig} Significant Wave Height of Infragravity Waves

H_k Transform Coefficient

H_{m0} Significant Wave Height

H_r Water Level

H_{ss} Significant Wave Height of Sea and Swell Waves

ρ Density

g Gravity

hrs Hours

h Water Depth

k Wavenumber

n Manning's Roughness Coefficient

P_n Hydrostatic Pressure Term

P_{nh} Non-Hydrostatic Pressure Term

τ_{xx}, τ_{xz}, τ_{zz}, τ_{zx} Turbulent Stresses

T_p Peak Wave Period

C_f Bottom Friction Coefficient

1D One-Dimensional

2D Two-Dimensional

Chapter 1

Introduction

Over the past decade, impacts associated with sea-level rise in vulnerable low-lying regions across the Pacific have increased the demand for timely and accurate predictions of coastal inundation. These intensifying demands are prompting institutions like the National Oceanic and Atmospheric Association's (NOAA) National Weather Service (NWS), which is responsible for warning coastal communities covering the state of Hawaii, American Samoa, Guam, the Federated States of Micronesia (FSM), the Republic of the Marshall Islands (RMI), and the Republic of Palau, to seek innovative solutions.

The Nearshore Wave Prediction System (NWPS, *Van der Westhuysen et al.* (2013)) run by the NWS's National Centers for Environmental Prediction (NCEP), features the phase-averaging Simulating WAves Nearshore (SWAN, *Booij et al.* (1999)) spectral wave model with a peak grid resolution down to hundreds of meters, which is too coarse for resolving wave transformations across the reef after breaking. Specifically, a more challenging factor is that most modeling component designs within the NWPS that address wave runup and inundation have been developed and tested for U.S. mainland coasts, which are characterized mainly by flat and broad bottom shelves and slopes with sandy beaches. However, recent advances in phase-resolving models and observational studies have improved the representation of wave and water-level interactions, showing that low-frequency oscillations from infragravity waves dominate water-level forecasts in reef environments (*Zijlema*, 2012). These models can capture the complex physics of wave transformation and dissipation in reef environments, which is not possible with the aforementioned traditional phase-averaging wave models and predictions that rely on empirically-derived formulations based on sandy beach profiles (*Stockdon et al.*, 2006) included within NOAA's NWPS.

Although there are several ongoing modeling efforts and support from the Department of Ocean and Resources Engineering at the University of Hawaii (UH-ORE) and the Pacific Island Ocean Observing System (PacIOOS) using phase-resolving models operationally, such as the Boussinesq Ocean and Surf Zone model (BOSZ, *Roeber and Cheung* (2012)), none of them are implemented within the NWS across the Pacific. This is a significant limitation operationally, where forecasters have to frequently provide decision support services to core partners within Ocean Safety and Emergency Management sectors regarding the potential for coastal inundation during extreme wave events each year.

This thesis addresses the gap between the computational demands of two-dimensional (2D) phase-resolving modeling platforms and their feasibility in an operational forecast environment within the NWS's Pacific Region. The primary objective is to conduct a comprehensive sensitivity study that presents the results of an evaluation using the Simulating WAves til SHore (SWASH, *Zijlema et al.* (2011)) phase-resolving model on the North Shore of Oahu, Hawaii. This study evaluates the sensitivity of the model's accuracy relative to bottom friction and spatial resolution versus computational time. The analysis results offer operational forecasters guidance on fine-tuning model settings and configurations to attain the desired precision while conserving computational resources and reducing computation time.

Implementing a phase-resolving model in operations like SWASH would be a monumental step forward for coastal locations within the NWS across the Pacific. The effectiveness of SWASH as a numerical model enables precise predictions across a wide range of future applications, including wave heights at the shore (shore break hazards) after transformation, wave-induced water levels, rip currents, wave runup, and inundation. Being close to the framework of SWAN, which is already heavily utilized within the NWS, the system could quickly become absorbed within the NWPS modeling platform centralized at NCEP.

The thesis is structured as follows: Chapter 2 gives an overview of the field observations in the literature and available operational guidance for reef-lined coasts. Chapter 3 discusses the SWASH model and the input parameters. Chapter 4 presents the sensitivity analysis and findings. Chapter 5 summarizes the conclusions and recommendations.

Chapter 2

Field observations and Numerical Modeling of Wave-Driven Inundation in Reef Environments

2.1 Field Observations

Reef-lined coasts present unique challenges in wave-driven water-level predictions, significantly differing from U.S. mainland coasts with sandy shores. Observational studies across the Pacific have shed light on these challenges, emphasizing the rapid changes in depth and the complex coastal shapes characterized by steep offshore slopes transitioning to varying widths over shallow reef flats. Additionally, irregularly-shaped deep channels further complicate water level dynamics in reef environments. This section discusses influential factors and parameters crucial for evaluating numerical water level predictions for island coasts, laying the groundwork for understanding extreme water-level forecasts during large wave events.

2.1.1 Wave Setup

Intense wave breaking observed at the reef edge associated with dispersive long-period swell events translates to increasing water levels shoreward of the reef due to wave setup. *Vetter et al.* (2010) confirmed this during a Pacific Island Land Ocean Typhoon (PILOT) experiment on the island of Guam. Similar wave-driven water level anomalies were observed over the Midway Atoll in a study by *Aucan et al.* (2012). They showed strong correlations between wave heights on the reef's edge and wave setup over the reef and within the interior Midway Atoll lagoon, based on the formulation of *Longuet-Higgins and Stewart* (1962). In a study from 2000, Massel and Gourlay (*Massel and Gourlay*, 2000) discussed how complex coastal shapes and variations in reef structures can induce large spatial gradients in sea level (wave setup or setdown). This occurs due to wave energy focusing in specific areas over the reef in response to nearshore wave transformations such as shoaling, refraction, diffraction, and dissipation processes.

2.1.2 Friction

Reef flats are often spatially inhomogeneous and offer various coral reef species and geomorphologies. These variations across the reef are correlated with either higher or lower rates of wave energy dissipation due to friction, which can attenuate energy as much as wave breaking. A two-week experiment on the Kaneohe Bay barrier reef on the island of Oahu in Hawaii showed that most wave energy dissipation is correlated to bottom friction, with wave breaking not being as significant (*Lowe et al.*, 2005). Similar results were shown on the north shore of Oahu by *Filipot and Cheung* (2012) using the nearshore wave model SWAN. Bottom friction is also found to play a role in low frequency motions on reef flats and during wave runup (*Zijlema*, 2012). In a study along the southern shores of Oahu, Hawaii from *Gerritson* (1981), friction coefficients for prototype conditions were established. These coefficients confirmed the significant role friction plays in dissipating wave energy in the breaking zone.

2.1.3 Infragravity Waves

Observations reveal non-linear interactions that translate to dynamic shifts in the spectral shape from incipient breaking to the shore during wave transformation, where the peak energy is transferred from the sea and swell (S-S, 0.04 to 0.2 Hz) frequency bands to the infragravity (IG, 0.04 to 0.005 Hz) bands (*Bertin et al.* (2018); *Munk* (1949) and *Tucker* (1950)). They also found that wave motions were dominated by these low frequency oscillations over the reef, whereas, the higher frequency (S-S) energy is diminished mostly at incipient breaking on the reef's edge.

2.2 Inundation Modeling Efforts for Reef-Lined Coasts

Although many approaches in the past have used a combination of empirically and semi-empirically derived methods to predict inundation associated with wave breaking, transformation across the reef, and the associated extreme water levels (*Massel and Gourlay* (2000); *Sheremet et al.* (2011); *Merrifield et al.* (2014); *Caldwell and Aucan* (2007)), more recent advances with phase-resolving wave models have emerged and been developed to more realistically simulate these nearshore processes. These models simulate amplitude and phase variation of S-S waves while using either the nonlinear shallow water (NLSW) equations (SWASH, *Zijlema et al.* (2011)) or the Boussinesq-type models (FUNWAVE, *Shi et al.* (2012), BOSZ, *Roeber and Cheung* (2012), and XBeach surfbeat (XB-SB, *Roelvink et al.* (2009))). These models directly account for wave transformations during extreme events, when the S-S energy is transferred to IG frequency bands following breaking.

The BOSZ modeling platform discussed above has been the foundation for many inundation-based modeling applications in the Pacific between the UH-ORE and PacIOOS. Over the past decade, this task group has developed an extensive array of operational forecast tools addressing coastal impacts ranging from wave-runup, high sea levels, harbor surges, and inundation risk maps (*Azouri* (2016); *Guiles et al.* (2019); *Roeber et al.* (2019); *Tognacchini* (2023)). The XB-SB modeling platform was used as a basis for developing a forecast system ("BEWARE": Bayesian Estimator for Wave Attack in Reef Environments) that estimates how different wave, water level, and reef combinations can lead to flooding (*Pearson et al.*, 2017) along low-elevation, coral reef-lined, tropical coasts. Although most operational applications use a one-dimensional (1D) approach due to computational constraints, the West Maui Runup model, as described in *Guiles et al.* (2019) and *Roeber et al.* (2019), represents a notable advancement with its implementation of a 2D grid configuration using the BOSZ model.

2.3 NOAA's Wave and Inundation Guidance

Due to computational complexities and other challenges, none of the phase-resolving or empirically-based models discussed in section 2.2 are available within NOAA's NWS Pacific Region. Forecasters within this region are entrusted with the responsibility of issuing coastal advisories, watches, and warnings that address coastal impacts associated with inundation. Given the operational requirement for rapid turnaround times of less than six hours, it is critical that these resources become available to operational forecasters to support their ability to properly message future impacts to coastal communities.

Van der Westhuysen et al. (2011) compiled a white paper summarizing these limitations in the Pacific within NOAA's Coastal Storms Program (CSP) effort that included a list of inundation guidance resources available at that time for these NWS forecast sites. This list included The Surge and Wave Island Model Studies tool (SWIMS, *Smith et al.* (2011)) and the Sea, Lake, and Overland Surges from Hurricanes (SLOSH, *Jelesnianski et al.* (1992)) model, which are forecasting systems that address coastal inundation impacts associated with tropical cyclones. For forecasts of inundation from extratropical cyclones, the Extra-tropical Surge and Tide Operational Forecast System (ESTOFS, *Funakoshi et al.* (2012)) had been developed for the east coast with the ADvanced CIRCulation storm surge model that was developed by *Luettich et al.* (1992) driving the water level and surge predictions across an unstructured grid. The NWPS was under development then, with plans to be centralized on NOAA's supercomputers. The phase-averaging spectral wave model SWAN is the primary modeling platform within the system with a maximum spatial resolution ranging from 100 m to 2 km. The model is initialized with the WAVEWATCH III® (WW3, *Tolman et al.* (2002); *Chawla et al.* (2013)) and applies water levels and ocean currents for wave-water level and wave-current interactions using the Real Time Ocean Forecast System (RTOFS, *Mehra and Rivin* (2010)) and ESTOFS in a loosely coupled system. Table 2.1 provides an overview of these modeling platforms described.

Table 2.1: Overview of numerical platforms being run in operations between academia and NOAA/NWS for Pacific Islands

Model	**Type**	**S-S**	**IG**	**Academia**	**NOAA**
BOSZ	Phase-resolving	Yes	Yes	UH-ORE/PacIOOS	No
FUNWAVE	Phase-resolving	Yes	Yes	Yes	No
XB-SB	Phase-resolving	Yes	Yes	Yes	No
SWASH	Phase-resolving	Yes	Yes	Yes	No
SWAN	Phase-averaging	Yes	No	Yes	Yes
WW3	Phase-averaging	Yes	No	No	Yes
SWIMS	Tropical Cyclones	Yes	Yes	Yes	Yes
SLOSH	Tropical Cyclones	Yes	No	No	Yes
ESTOFS	Tide/Water Level/Surge	No	No	No	Yes
RTOFS	Currents	No	No	No	Yes

2.4 Bridging the Gap between Research and Operations

NOAA's NWS field offices across the Pacific are responsible for many Pacific Islands and face significant challenges when addressing coastal impacts associated with extreme water levels observed. Consequently, forecasters at these NWS locations lack proper guidance that addresses these field observations when forced to provide decision-support services to core partners. This problem is further compounded due to the growing challenge associated with sea level rise, which translates to an increasing frequency of wave-induced inundation events. Our goal is to establish a concise set of guidelines that allow operational forecasters to balance a model's expected accuracy against computational expense.

Chapter 3

Methodology

3.1 SWASH Overview and Description

The SWASH model is a non-hydrostatic wave-flow model intended to numerically resolve wave transformations over shallow nearshore waters in 1D and 2D (*Zijlema et al.*, 2011). This model was developed by the Environmental Fluid Mechanics Section of the Faculty of Civil Engineering and Geosciences at The Delft University of Technology (*The SWASH Team*, 2023). The governing equations are the nonlinear shallow water equations, including the non-hydrostatic pressure term (*Smit et al.*, 2013):

$$\frac{\partial u}{\partial t} + \frac{\partial (uu)}{\partial x} + \frac{\partial (uv)}{\partial y} + \frac{\partial (\omega u)}{\partial z} = -\frac{1}{\rho}\frac{\partial (Pn + Pnh)}{\partial x} + \frac{\partial \tau_{xz}}{\partial z} + \frac{\partial \tau_{xx}}{\partial x} \tag{3.1}$$

$$\frac{\partial v}{\partial t} + \frac{\partial (uv)}{\partial x} + \frac{\partial (vv)}{\partial y} + \frac{\partial (\omega v)}{\partial z} = -\frac{1}{\rho}\frac{\partial (Pn + Pnh)}{\partial y} + \frac{\partial \tau_{yz}}{\partial z} + \frac{\partial \tau_{yx}}{\partial x} \tag{3.2}$$

$$\frac{\partial \omega}{\partial t} + \frac{\partial (u\omega)}{\partial x} + \frac{\partial (v\omega)}{\partial y} + \frac{\partial (\omega\omega)}{\partial z} = -\frac{1}{\rho}\frac{\partial Pnh}{\partial z} + \frac{\partial \tau_{zz}}{\partial z} + \frac{\partial \tau_{zx}}{\partial x} \tag{3.3}$$

$$\frac{\partial u}{\partial x} + \frac{\partial v}{\partial y} + \frac{\partial \omega}{\partial z} = 0 \tag{3.4}$$

η is the free surface elevation - (u(x,y,z,t)), v(x,y,z,t) and ω(x,y,z,t) are the horizontal and vertical velocities - ρ is the density of water - h is the water depth - P_n and P_{nh} are the hydrostatic and non-hydrostatic pressures - and τ_{xx}, τ_{xz}, τ_{zz} and τ_{zx} are the turbulent stresses. These equations provide a general basis for describing complex changes to rapidly varied flows typically found in coastal flooding resulting from, e.g., dike breaks and tsunamis, and wave transformation in both surf and swash zones due to nonlinear wave–wave interactions, the interaction of waves with currents, and wave breaking as well as runup at the shoreline (*Zijlema et al.*, 2011). In principle, SWASH has no limitations and can capture flow phenomena with spatial scales from centimeters to kilometers and temporal scales from seconds to hours (*The SWASH Team*, 2023).

3.2 SWASH vs. Boussinesq-Type Wave Models

SWASH improves its frequency dispersion by increasing the number of layers rather than increasing the order of derivatives of the dependent variables like Boussinesq-type wave models (*The SWASH Team*, 2023). Since the importance of nonlinearity increases as the depth decreases and waves begin to shoal, strong vertical gradients in the particle velocities arise in the upper portion of the column near breaking (*Smit et al.*, 2013). These strong gradients require many vertical layers (higher vertical resolution) to effectively resolve the flow in the upper column and near the wave crests within the surf zone. However, this requirement to increase the vertical resolution would be prohibitive in an operational setting due to the added computational expense. To counter the necessity for many layers vertically, *Smit et al.* (2013) developed a hydrostatic front approximation similar to turning off the dispersive terms in the Boussinesq equations (*Tissier et al.*, 2012). This approximation ensures that the wavefront rapidly devolves into a bore-like structure after breaking, even with a few layers (i.e., 1-3) employed in the simulations. This added functionality provides a more feasible and economical solution computationally.

3.3 Low-frequency Oscillations in Reef Environments

As detailed in Chapter 2, observations in reef-lined environments underscore the significance of low-frequency oscillations within the IG bands across the reef flat, particularly their dominance near the shore during highly energetic wave events. Zijlema et al. (2012) demonstrated, through employment of SWASH, the generation and propagation of this phenomenon across fringing reefs. Their findings concluded that the model captured both the amplitude and phase of the IG oscillations over the reef flat, highlighting how low-frequency motions amplify in instances of reduced water levels over the reef flat.

3.4 Model Time Integration

In contrast to phase-averaging models, such as SWAN (*Booij et al.*, 1999), where action density limiters and implicit propagation schemes are used to maintain numerical accuracy and stability with large time steps violating the Courant-Friedrichs-Lewy (CFL) stability criteria, SWASH requires strict adherence of the CFL criterion. This compliance is necessary for ensuring a stable solution through explicit time integration (*Zijlema et al.*, 2011). This time step is dynamically adjusted throughout the simulations depending on the evaluation of the CFL number at each node for 2D simulations, which is defined in the manual (*The SWASH Team*, 2023) as:

$$Cr = \Delta t \left(\sqrt{gd} + \sqrt{u^2 + v^2} \right) \sqrt{\frac{1}{\Delta x^2} + \frac{1}{\Delta y^2}} \leq 1 \tag{3.5}$$

where g represents the acceleration due to gravity, d reflects the water depth, Δx and Δy denote the mesh width, Δt stands for the time step, u and v represent the flow velocity, and Cr signifies the Courant number. For this study, the Cr-min is 0.1, and the Cr-max will dynamically change depending on the type of scenario that evolves based on the given boundary conditions (advised default = 0.5).

3.5 Model Version and Physics

The sensitivity analysis presented in this study was produced using the SWASH model, version 6.01. The following settings for the model simulations and physics were applied:

- Energy dissipation through wave breaking is accounted for with $\alpha = 0.6$ (25° slope along the wave face), which represents the maximum local surface steepness and determines the onset of the breaking process defined by *Lynett* (2006).

- Sommerfeld radiation condition is employed, which minimizes reflections of long waves at the opposite side of the computational grid that was initialized with boundary conditions (wave height and period).

- The bottom friction coefficient was calculated from the Manning's roughness coefficient n ranging from 0.019 (SWASH default; smooth) to 0.2 (very rough), as follows:

$$C_f = \frac{n^2 g}{\sqrt[3]{h}} \tag{3.6}$$

  (h is the water depth)

- The shape of the spectra (both in frequency and direction) at the boundary of the computational grid was defined with the JONSWAP spectrum, with $\lambda = 3.3$.

- Non-hydrostatic pressure is activated in the shallow water equations with the default Keller-Box scheme for the pressure gradients in the vertical momentum equations.

3.6 Computational Grid Setup

The size of the computational grid developed extends 12 km in the x-direction (alongshore) and 9 km in the y-direction (cross-shore). This 2D grid is rectilinear (uniform), meaning the width between each column is preserved in the x- and y-direction and vertically bounded within one layer (i.e. depth-average mode) between the free surface and underlying topography. The x-axis extending from the computational grid origin was rotated 40 degrees in the horizontal plane due to the orientation of the coast, which minimized the number of dry grid cells in the computation domain.

Simulations in this study were conducted using the Keller-Box scheme, which should provide good dispersive properties given the aforementioned coarse vertical resolution consisting of one layer ($kd < 2.9$ – k being the wavenumber and d the depth) (*Zijlema et al.*, 2011). Given the domain size in geographical space, the Cartesian coordinate system was used with an origin positioned at (0,0). To prevent wave reflections at the open boundaries throughout the simulations, sponge layers were implemented along the eastern and western sides to effectively absorb outgoing wave energy. In addition to the 2D grid defined, 1D simulations were performed along a transect extending seaward through the grid point that will be evaluated throughout the sensitivity tests.

3.7 Input Sources

Bathymetric-topographic input to the SWASH grids was taken from various digital elevation models (DEMs) configured by the National Geophysical Data Center (NGDC). The one-third arc-second (10 m horizontal grid spacing) gridded Digital Elevation Model (DEM) of Oahu, Hawaii (*NGDC*, 2011) referenced to Mean High Water (MHW) was the primary database used. This DEM included 168 NGDC multibeam sonar surveys, three National Ocean Survey (NOS) high-resolution surveys in Bathymetric Attributed Grid (BAG) format, and 10 Electronic Nautical Charts (ENCs) that were available from OCS (*NGDC*, 2011). The dataset used to build the Oahu DEM included 29 high-resolution coastal lidar surveys from the USACE Scanning Hydrographic Operational Airborne Lidar Survey (SHOALS) Coastal Topography-Bathymetry Lidar (*NGDC*, 2011).

The influence of water levels on the wave field is considered only in terms of adding to or reducing the still water depth defined from the bathymetric-topographic database. These water level deviations resemble the local tides observed in the test region and relative to the vertical MHW datum. These changes to the still water level were static, meaning no temporal component resembling a typical tidal time series was included, due to the short duration of the test cases (less than 3-hrs).

The wave boundary conditions are applied as input along the seaward side of the grids, which are aligned with the coast and consist of a nearly uniform depth. Peak wave direction is shore-normal due to the proximity of the reef face. The assigned significant wave height and peak period are modulated through the generation of irregular sea states based on the JONSWAP spectrum with a peak enhancement factor of 3.3 (the SWASH default). A weakly reflective boundary is applied at the wave boundary, and the Sommerfeld radiation condition is applied at the end of the numerical domain, in order to minimize the effect of the reflection.

Chapter 4

Sensitivity Analysis

4.1 Overview

The following evaluation aims to determine the level of sensitivity to various numerical settings and grid configurations when employing the spectral wave model SWASH discussed in Chapter 3. It also aims to evaluate the computational expenses involved, which is useful information for operational forecast offices within NOAA's NWS that require quick model return times. This evaluation entails determining the level of sensitivity by varying the influential parameters previously identified in Chapter 2, through experimentation with idealized boundary conditions and water levels. These input variables include simulation time, bottom friction, dimensionality, and the computational cost as a function of resolution. Output parameters computed from the simulated surface elevations used to assess model performance are the two-percent exceedance wave height ($\eta_{2\%}$), wave setup (η_s), sea and swell height (H_{ss}), and infragravity wave height (H_{ig}). Figure 4.1 summarizes these variables and grid configurations discussed in the following sections.

4.2 Study Area and Seasonal Climatology

The numerical evaluation is performed along the North Shore of Oahu, Hawaii, from Ke Iki Beach to Kawela Bay, which is shown in Figure 4.2. This nine-kilometer stretch of the

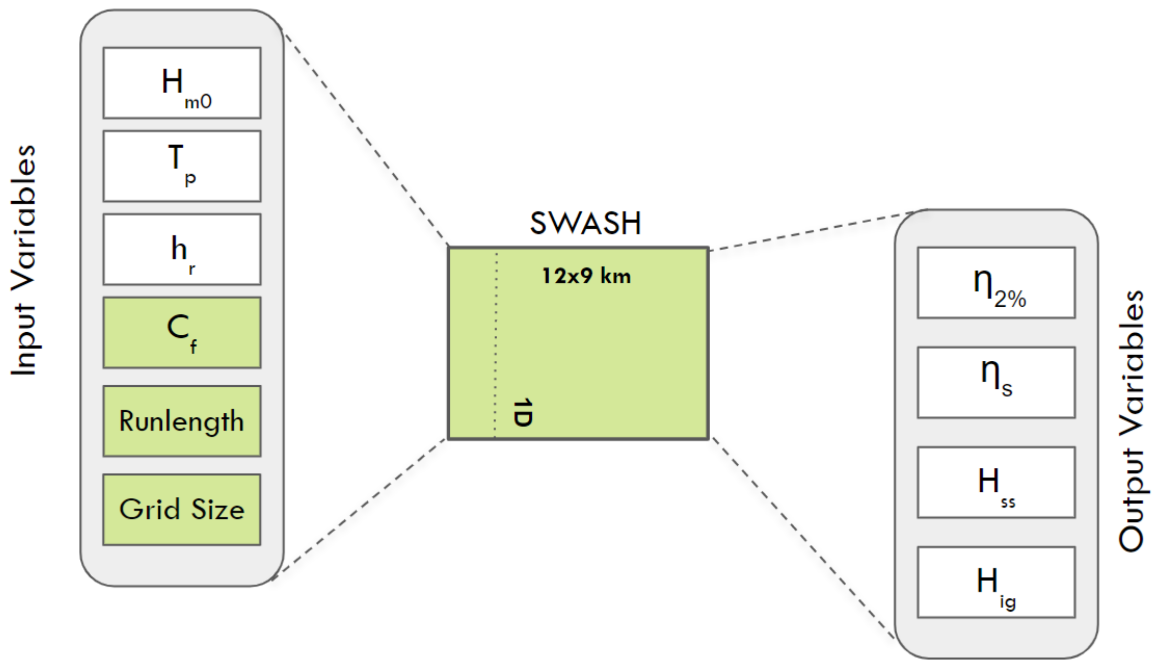

Figure 4.1: Input variables include simulation time (Runlength), bottom friction (C_f), dimensionality (2D vs. 1D), and resolution (grid size) while varying wave height (H_s), peak wave period (T_p) and water levels (h_r). Bulk-averaged output parameters computed from the simulated surface elevations from each test that are used to assess model performance include the two-percent exceedance wave height ($\eta_{2\%}$), wave setup (η_s), sea and swell height (H_{ss}), and infragravity wave height (H_{ig}).

coast faces northwest (320-330 degrees) and generally consists of a gently sloping fringing reef offshore, with limited modern reef growth (*Fletcher et al.*, 2008). *Franklin et al.* (2013) used statistical distribution models to estimate coral distribution based on various factors in this region, such as wave climatology. They found coral coverage percentages generally less than 30 percent. Large fluctuations in beach profiles ranging from very wide beaches in the summer to narrower and steeper beaches through the winter months due to the high frequency and duration of energetic swell and surf events were shown by *Walker* (2017). Large winter swell events regularly impact the shorefront infrastructure adjacent to these beaches. Impacts include water sweeping over beaches that typically remain dry, significant beach erosion undercutting coastal properties, and overwashing onto the coastal highway that impedes traffic flow.

The location of the Hawaiian Islands in the central Pacific and proximity to the northern Pacific winter storms translates to frequent extreme wave events between September and May annually. Wave transformation from the deep to shallow waters is characterized by amplification around the reef face due to a combination of the low-frequency swell energy and the steep and narrow slopes at the reef face. The Goddard-Caldwell database (*Caldwell*, 2005) (hereafter GCD) - a 55-year running observational surf height database (1968-present) within the study area—documents the seasonal climatology, showing a seasonal peak centered on January. Statistical analysis of the GCD in various surf-height bands produces a mean of 51 days per winter season when surf heights range from five to eight meters (19 %), 16 days when surf heights range from eight to 12 meters (6 %), and four days (2 %) when the surf heights exceeded 12 meters (2 %). These trends correlate well with wave observations from a nearshore wave buoy, positioned around five kilometers off the coast at a depth of 200 m, made available by the PacIOOS and the CDIP in partnership with the Department of Oceanography at the University of Hawaii.

Water levels in the Hawaiian Islands are influenced mostly by a mixed semidiurnal tide cycle, with a diurnal tidal range of around 50 cm. Extreme tides occasionally exceed

30 cm above the Mean Higher High Water (MHHW) datum, usually occurring late at night or through the early morning hours around or before daybreak during the winter months. Although minor coastal flooding impacts are observed when these extreme water levels occur with or without waves (still water-level anomalies alone), the impacts are exacerbated when high water levels coincide with large swell and surf events, which are cataloged in *Caldwell et al.* (2009).

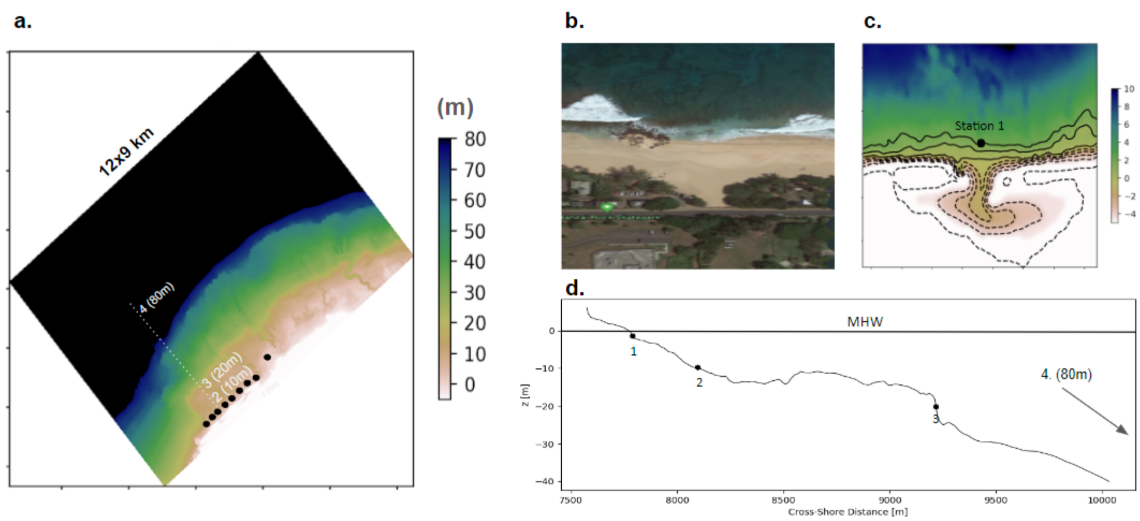

Figure 4.2: (a) Location of the study site at Rock Piles Beach and bathymetric overview on the North Shore of Oahu. (b) A view of the vulnerable low-lying coastal highway and beach at Rock Piles. (c) A spatial overview of the bathymetry at Rock Piles and locations of the street and the point (Station 1) at a depth of 2 m that was used to evaluate the SWASH output. (d) Topography along the cross-shore transect at Rock Piles with the location and station number of the points (circles) that will be used to evaluate the computed SWASH output.

4.3 Analysis methods

For each simulation, a time series of the computed surface elevations at critical points across the reef and along the 2 m isoline is output with a sampling interval (δt) of one second through the duration of the simulations. Only the time series' final 900 seconds (cycle time = 15 minutes) are used to compute how the wave energy is distributed within individual frequency bands throughout the spectrum by performing a discrete Fourier transform (DFT).

Frequencies, power spectrum (PS), and power spectral density (PSD) are calculated from the time series. To minimize the noise in the raw periodogram and suppress spectral leakage, a simple boxcar smoothing function is applied at the cost of sacrificing resolution in frequency space. Figure 4.3 depicts the result of a smoothed periodogram, along with a grey shaded region representing the 95% confidence intervals. This demonstrates the use of the smoothing boxcar approach in reducing noise and suppressing spectral leakage, while the confidence intervals show the level of uncertainty surrounding the spectral density estimates. For the PS, the Fourier Transform coefficients (H_k) are divided by the square of the number of 1-sec values (N^2) using Parseval's Theorem by

$$\frac{1}{N^2}\sum_j |h_j|^2 = \frac{1}{N^2}\sum_k |H_k|^2 \tag{4.1}$$

where h_j are the given points through the time series. For the PSD, the PS is multiplied by the record length,

$$L = N\Delta t, \tag{4.2}$$

and the interval between the frequencies is,

$$\Delta f = \frac{1}{L} \tag{4.3}$$

in cycles per second. Variance within a desired frequency range is obtained by integrating the area under the PSD curve between two frequencies, f_1 and f_2:

$$\int_{f_1}^{f_2} PSD\, df \tag{4.4}$$

For this analysis, bulk-averaged output parameters, including the significant sea and swell height (H_{ss}: 0.2 to 0.04 Hz), and infragravity wave height (H_{ig}: 0.04 to 0.001 Hz) are computed from the spectral variance of the free surface displacement accordingly:

$$H_{ss} = \sqrt[4]{\int_{0.04}^{0.2} PSD\, df} \tag{4.5}$$

$$H_{ig} = \sqrt[4]{\int_{0.001}^{0.04} PSD\, df} \tag{4.6}$$

Wave setup (η_s) is computed by taking the average of surface elevations through the 15-minute cycle period at the desired output points. The two-percent exceedance height ($\eta_{2\%}$) is calculated by finding the 98th percentile, which means the probability of the computed value being exceeded is two percent or less. The NumPy library used to define percentiles sorts the data in ascending order, then computes an index of the value at the desired percentile using the formula:

$$i = \left(\frac{p}{100}\right) \cdot (n-1) + 1 \tag{4.7}$$

where p is the percentile, n is the number of values in the data set, and i is the index of the value at the desired percentile. Once the index is established, the percentile value is computed through linearly interpolating between the nearest neighbors to the index. Table 4.1 summarizes these bulk parameters and their separation frequencies.

Table 4.1: Parameters evaluated throughout the analysis.

Output Parameter	Symbol	Frequency
Sea and Swell Height	H_{ss}	0.2 - 0.04
Infragravity Wave Height	H_{ig}	0.04 - 0.001
Wave Setup	η_s	-
Two-percent Exceedance Height	$\eta_{2\%}$	-

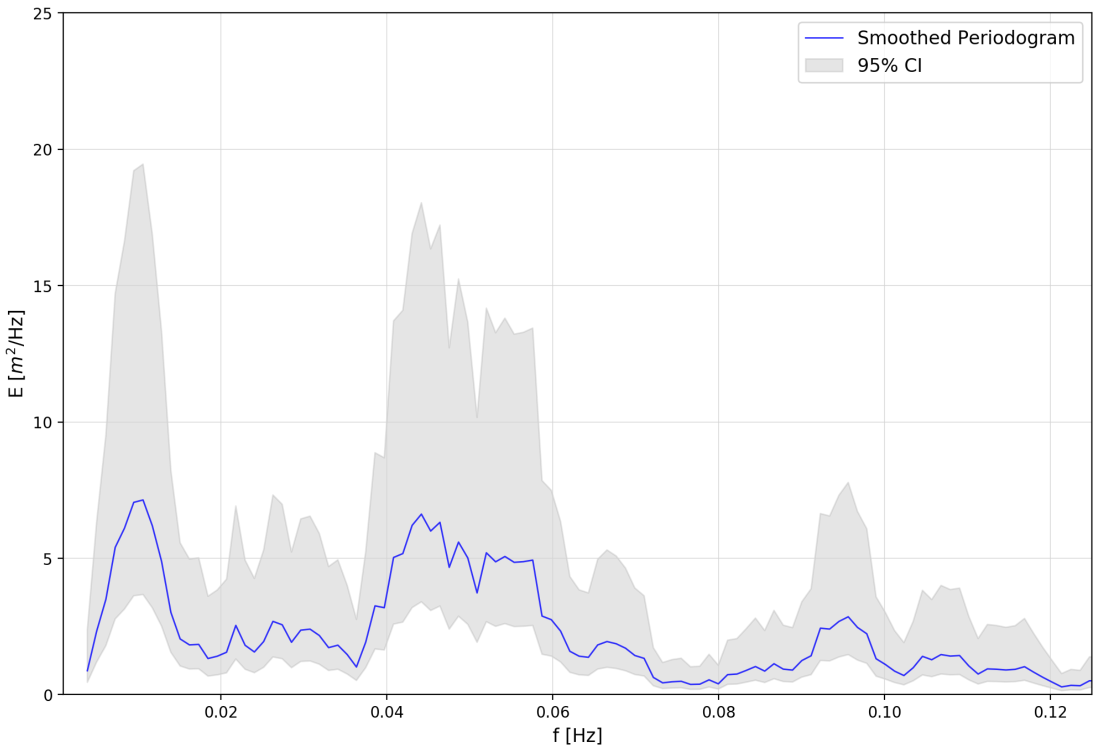

Figure 4.3: Illustrates the spectral analysis of a data sample. To mitigate the noise from the raw periodogram, a moving average (blue line) is applied, resulting in a smoothed periodogram. The smoothing process involves averaging the spectral density over 6 adjacent frequency bands, corresponding to a width of approximately 0.006 Hz. The grey shaded region represents the 95% confidence interval (CI), indicating the level of uncertainty in spectral density estimates across the spectrum.

4.3.1 Performance Assessment and Metrics

The performance of each test is evaluated by comparing the ratio of the difference between the model test results (φ_{mod}, $\eta_{2\%}$, η_s, H_{ss}, and H_{ig}) and the reference results (φ_{ref}, $\eta_{2\%}$, η_s, H_{ss}, and H_{ig}) to the reference results times 100 to obtain the percent difference at a defined output point, namely

$$PercentDifference_{\varphi} = \frac{\varphi_{\text{mod}} - \varphi_{\text{ref}}}{\varphi_{\text{ref}}} \times 100 \tag{4.8}$$

The reference model configuration used throughout the tests is defined with a three-meter resolution over a 2D grid (12-km by 9-km - 12 million grid points) and a model simulation time of four hours, as highlighted in Table 4.2 in the following section. Although this reference configuration is not attainable in an operational environment due to computational constraints, it was chosen to ensure stable numerical results. This decision was driven by the need for a reliable baseline for comparison, given the absence of real-time observations in the region during the sensitivity evaluation. This reference test serves as a benchmark, representing the best configuration attainable within our computational resources for model validation and comparison purposes. For operational applications, a margin error of 10% or less between the tests and this reference simulation is considered acceptable.

The bulk parameters computed from the surface elevations are evaluated and compared at four points along the transect shown in Figure 4.2 (d.) ranging from an offshore location (80 m) near the grid boundary, reef face (20 m), reef flat (10 m), near the toe of the beach (2 m), and at nine output locations along 2 m isoline. Results depicting a negative percent difference reflect a low bias for the model test, while a positive difference reflects a high bias.

4.4 Test Cases

Table 4.2 summarizes 47 test cases highlighting various combinations of model input conditions that will be used in the following sections to evaluate model sensitivity. As an attempt to reproduce conditions that are typically observed in this region, breaker heights (H_b) and water levels (h_r) corresponding to real-time cases were taken from *Caldwell* (2005), where events were categorized by severity (ranging from marginal to extreme) through qualitative assessment of reported coastal impacts. Since the cataloged surf heights per event from this work cannot be directly applied in SWASH as boundary forcing, observed swell heights (H_{m0}) at a nearby directional PacIOOS wave rider buoy (Waimea Bay; station 51201) and peak periods (T_p) that match event times cataloged in *Caldwell and Aucan* (2007) were applied. Initial conditions for stillwater level in the SWASH simulations ranged from what is typically observed at high tides to extreme high tides.

4.5 Model Simulation Time

Operational settings must find a balance between accuracy and efficiency, and simulation time is an essential consideration for efficiency. In general, numerical wave-transformation models like SWASH require spin-up time for the model solutions to converge and stabilize. To assess whether a SWASH simulation has reached a steady state, meaning the solutions have stabilized and will not change significantly with longer simulation times, a model time convergence test is an integral stage to consider for an initial grid setup. This is a critical step because SWASH requires a significant amount of computational time and resources to run, and a model that has not converged will not produce consistent results.

Factors that must be accounted for when determining an optimal simulation time for a new grid include domain size, the orientation of the coast relative to the wavemaker boundary, and the wave characteristics (low vs. high-frequency waves) that typically necess-

Table 4.2: Input conditions for the test cases evaluated.

Test Type	No.	Hmo (m)	Tp (s)	hr (cm)	Cf	Simulation Time (s)	Res. (m)
Ref. Sim.	1	2.5	18	75	0.035	14400	3
	2	3.5	18	25	0.035	14400	3
	3	3.0	18	75	0.035	14400	3
	4	3.0	18	50	0.035	14400	3
Sim. Time	1	3.5	18	25	0.035	900	3
	2	3.5	18	25	0.035	1800	3
	3	3.5	18	25	0.035	7200	3
Friction	1	2.0	18	25	0.019	7200	5
	2	2.0	18	25	0.035	7200	5
	3	2.0	18	25	0.050	7200	5
	4	2.0	18	25	0.065	7200	5
	5	2.0	18	25	0.080	7200	5
	6	2.0	18	25	0.100	7200	5
	7	2.0	18	25	0.125	7200	5
	8	2.0	18	25	0.150	7200	5
	9	2.0	18	25	0.175	7200	5
	10	2.0	18	25	0.200	7200	5
2D vs. 1D	1	2.0	18	25	0.035	7200	5
	2	2.0	18	75	0.035	7200	5
Eff./Cost	1	2.5	18	75	0.035	7200	3
	2	3.5	18	25	0.035	7200	3
	3	3.0	18	75	0.035	7200	3
	4	3.0	18	50	0.035	7200	3
	5	2.5	18	75	0.035	7200	5
	6	3.5	18	25	0.035	7200	5
	7	3.0	18	75	0.035	7200	5
	8	3.0	18	50	0.035	7200	5
	9	2.5	18	75	0.035	7200	8
	10	3.5	18	25	0.035	7200	8
	11	3.0	18	75	0.035	7200	8
	12	3.0	18	50	0.035	7200	8
	13	2.5	18	75	0.035	7200	10
	14	3.5	18	25	0.035	7200	10
	15	3.0	18	75	0.035	7200	10
	16	3.0	18	50	0.035	7200	10
	17	2.5	18	75	0.035	7200	12
	18	3.5	18	25	0.035	7200	12
	19	3.0	18	75	0.035	7200	12
	20	3.0	18	50	0.035	7200	12
	21	2.5	18	75	0.035	7200	15
	22	3.5	18	25	0.035	7200	15

Test Type	No.	Hmo (m)	Tp (s)	hr (cm)	Cf	Simulation Time (s)	Res. (m)
Eff./Cost	23	3.0	18	75	0.035	7200	15
	24	3.0	18	50	0.035	7200	15
	25	2.5	18	75	0.035	7200	20
	26	3.5	18	25	0.035	7200	20
	27	3.0	18	75	0.035	7200	20
	28	3.0	18	50	0.035	7200	20

itate coastal impacts in a region. For this section of the coast in Hawaii, the optimal simulation time chosen will be based on the results from a convergence test applying low-frequency swell energy as the forcing at the wavemaker boundary.

For our 2D domain used throughout this sensitivity analysis (domain size: 12 km x 9 km), an irregular spectrum centered around a low-frequency swell (Tp = 18 seconds) applied takes around 400-450 seconds before the first wave reaches the shore from the wavemaker boundary. This equates to around 200 to 300 waves every 3600 seconds of simulation time. For a suitable simulation time, the SWASH manual suggests at least 500 to 1000 waves are needed before a steady state is reached. This equates to an optimal simulation time of around two hours.

4.5.1 Model Convergence Time Window

Figure 4.5 quantifies how strongly the simulation time can influence the model output along the 2 m contour (nine output locations shown along the contour from west to east: X-axis 0-8) for $\eta_{2\%}$ (top left), η_s (top right), H_{ss} (bottom left), and H_{ig} (bottom right), with percent differences decreasing as the simulation time increases. Significant low biases are highlighted for a simulation time of 900 seconds, where percent differences plunged into the -75 to -90 percent range for each parameter. Biases in the 1800-second simulation, while vastly improved from the 900-second results, remain highly variable along the contour and, in some cases, yield differences greater than the desired 10% margin of error. The accuracy trade-off is between 1800 seconds and a two-hour simulation, where strong convergence is shown. The mean biases in the bulk parameters strongly converged from the 1800-second to the two-hour simulation, where less than a 1% bias was shown for the two-hour simulations. Biases shown for the 1800-second simulation ranged from approximately -33% to 2% between the output parameters, which falls outside of the 10% margin of error targeted. Table 4.3 also highlights these biases explicitly and confirms strong convergence between 1800-second and two-hour simulations.

Since the output along the 2 m contour depicts strong convergence for simulation times greater than 1800 seconds, this analysis will focus on two-hour simulations. This choice is primarily practical since the purpose of this work is to strike a balance between accuracy and efficiency.

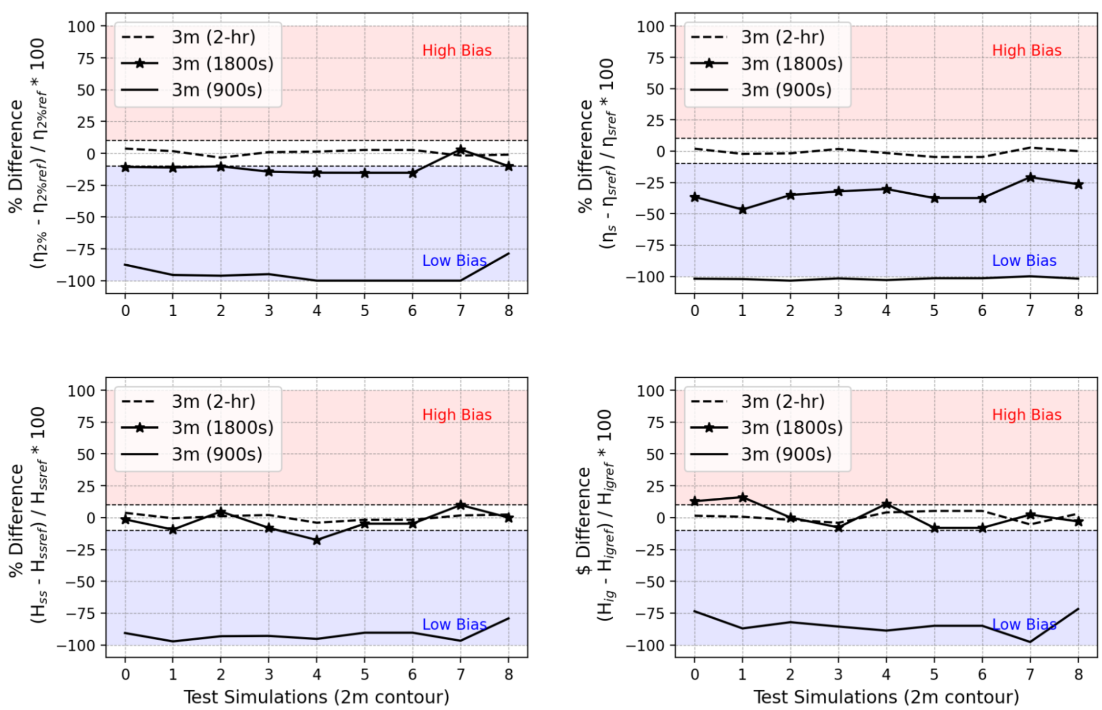

Figure 4.4: Percent differences are shown at nine (X-axis; 0-8, from west to east) output points along the 2 m contour between the model test and the reference simulation for $\eta_{2\%}$ (top left), η_s (top right), H_{ss} (bottom left), and H_{ig} (bottom right). Dashed horizontal lines bounding the white shaded region correspond to the ± 10% margin of error, where higher than 10% depicts a high bias and less than -10% depicts a low bias.

Table 4.3: Mean Biases (%) along the 2 m Isoline

Output Parameter	900s	1800s	2hr
2% Exceedance Height ($\eta 2\%$)	-94.742	-11.038	0.737
Wave Setup (η_s)	-101.932	-33.672	-0.941
Sea and Swell Height (H_{ss})	-91.768	-3.503	0.303
Infragravity Wave Height (H_{ig})	-84.05	1.673	0.918

4.6 Energy Dissipation due to Bottom Friction

Bottom roughness in a reef environment may dissipate as much energy as wave breaking and plays an essential role in low-frequency oscillations on reef flats (*Zijlema et al.*, 2011). Since determining bottom roughness is challenging and typically requires dedicated empirical investigation, testing the model sensitivity to dissipative processes, such as bottom friction, is important during initial implementation for an operational forecast office. This section aims to demonstrate the sensitivity of SWASH output at the shoreline to the bottom roughness factor using idealized test cases outlined in Table 4.2.

4.6.1 Bottom Friction Formulation in SWASH

We apply the Manning formulation of bottom friction for all tests presented in this study since it better represents wave dynamics in the surf zone than other formulations (*Zijlema et al.*, 2011). The dimensionless friction coefficient C_f is determined from Manning's roughness coefficient n, as follows:

$$C_f = \frac{n^2 g}{\sqrt[3]{h}} \tag{4.9}$$

where h is the local water depth. Robert Manning developed the roughness coefficient n, first appearing in Manning's paper 'On the flow of water in open channels and pipes' in

1891 (*Manning*, 1891). The empirically derived roughness factor (Manning's n) is well documented in the literature and can vary greatly depending on the type of bed surface. Example values of Manning's n coefficient for various surface types are shown in Table 4.4. The left column describes the surface characteristics, and along the right are the associated empirically-defined values. Values of n range from a smooth 0.02 for open water to 0.04 to 0.06 for bare rock or sand and a gravel pit.

Table 4.4: Typical Values of Manning's n

Surface Type	n
Open Water	0.020
Ice/Snow	0.022
Pasture	0.033
Commercial	0.050
Bare rock/sand	0.040
Gravel pit	0.060
Fallow	0.032
Transitional	0.100
Deciduous forest	0.160
Evergreen forest	0.180
Mixed forest	0.170
Shrub land	0.070
Grassland	0.035
Low residential	0.120
High residential	0.121
Row crops	0.040
Small grains	0.035
Recreational grass	0.030
Woody wetland	0.140
Herbaceous wetland	0.035

Although objective methods have been established to determine Manning's n based on physical properties of the surface for modeling applications, simulations over areas with large spatial variabilities and surface irregularities (large sandy areas, cuts in the reef, and varying density distributions of coral species), such as those found in fringing reef environments, introduce significant challenges and increase the likelihood of numerical inaccuracies. *Cialone and Smith* (2007) confirms the importance of considering bottom roughness variability over the southeast coast of Oahu, Hawaii, when validating output from a wave transformation model. They found that a spatially varying roughness factor for Manning's n ranging from 0.02 over the open waters seaward of the reef to 0.2 across the reef to the beach was an optimal solution during a validation experiment comparing model output to in-situ measurements.

This section aims to assess how strongly Manning's n influences the output from SWASH simulations. Results from this section will then be used as a baseline sensitivity to compare subjective model configuration choices (dimensionality, resolution, etc.) in subsequent sections. Model solutions presented in this section are based on simulations with a constant Manning's n applied across the model domain, with Manning's n ranging from 0.019 (smooth; SWASH default) to 0.2 (very rough; found by *Cialone and Smith* (2007) for southeast Oahu, Hawaii).

4.6.2 Model Sensitivity to Manning's n Along a Transect

Before evaluating the output along the 2 m isoline while varying Manning's n factor, it's necessary to determine where the sensitivity is highest as the waves propagate across the reef. To do this, we show the results of the computed spectra in Figure 4.5 from three of the ten test cases for friction presented in Table 4.5 at locations along a transect shown in Figure 4.2 (d). These three cases include values of Manning's n ranging from 0.2 (very rough) to 0.1 (rough) to 0.035 (smooth). As the waves propagate over the reef, each test shows the energy shifting from the spectral peak associated with the swell applied at the wavemaker boundary to the lower frequency IG bands near the coast. It's important to note that these test results are specific to the conditions of this study and is not a generalization. Similarily, the behavior of wave energy shifting to other frequency bands may vary under different scenarios. These tests reveal the sensitivity growing across the reef toward the shore during the wave transformation process, ranging from very little sensitivity seaward of the reef (top left panel) to highly sensitive at the 2 m output point (bottom right panel). At the 2 m output point, the energy within the IG bands becomes the dominant portion of the spectrum, especially for the smaller Manning's n values applied. The 95% confidence interval reveals this with a statistically significant spectral peak centered within these IG bands around 0.01 Hz. Additionally, the 0.035 Manning's n test showed a spectral peak slightly greater than the 95% confidence interval shaded region, indicating a solution outside of the expected spectral distribution for this test case. Similar results are shown over the reef at the 10 m output point.

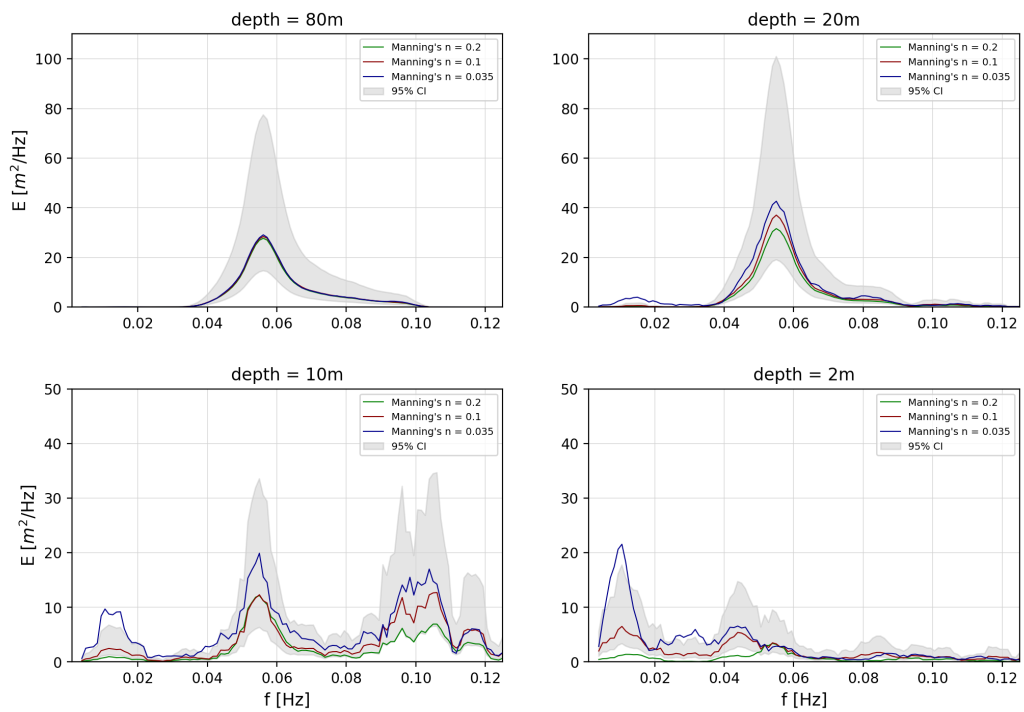

Figure 4.5: Comparison of computed spectra along a transect for three simulations varying the Manning's n for: 1) a point seaward of the reef (top left panel; 80 m depth), 2) reef face (top right panel; 20 m depth), 3) reef flat (bottom left; 10 m depth), and 4) near the toe of the beach (bottom right; 2 m depth). The 95% CI is only applied to the Manning's n test of 0.1, for clarity.

Table 4.5 quantifies the differences within the defined IG band and depicts a reduction of 36% (0.72 m band height) from the test using a Manning's n of 0.035 to 0.1 and a 71.5% (1.4 m band height) reduction from the test using a Manning's n of 0.035 to 0.2. Provided the sensitivity found near the shore along this transect, the following section will determine if a similar level of sensitivity is reflected along the 2 m contour.

Table 4.5: Wave height (m) comparisons between different roughness factors.

Dimension	Depth	Manning's n	$\eta_{2\%}$	η_s	H_{ss}	H_{ig}
$\Delta x, \Delta y$	2 m	0.035	1.83	0.27	1.80	1.96
$\Delta x, \Delta y$	2 m	0.1	1.57	0.27	1.71	1.24
$\Delta x, \Delta y$	2 m	0.2	0.2	-0.01	1.13	0.56

4.6.3 Model Sensitivity to Mannings's n at a Point along the 2 m Isoline

Since the strongest sensitivity was shown near the shore in section 4.6.2, after wave transformation, this section will investigate the level of sensitivity further at a point along the 2 m isoline using the 10 test cases varying Manning's n ranging from 0.019 (the SWASH default) to 0.2 shown in Table 4.2. Figure 4.2 (b. and c.) shows an overview of the test location (left) and the underlying topography (right) with the output point (Station 1) along the 2 m isoline labeled. This location is near Rock Piles Beach, where coastal impacts associated with wave runup and overwash typically occur.

Figure 4.6 demonstrates how strongly the Manning's n coefficient chosen can influence the model output after wave transformation at Station 1 for $\eta_{2\%}$ (top left), η_s (top right), H_{ss} (bottom left), and H_{ig} (bottom right), with percent differences decreasing as Manning's n increases. Although the slope is relatively steep for each of the bulk parameters shown in each panel, indicating the model is highly sensitive to friction, the steepest slope is depicted within the IG band height (bottom right). Here, the percent differences between the tests varying Manning's n and the reference simulation using 0.035 for Manning's n rapidly drop from around 10% using the SWASH default of 0.019 to around -22% for the test using 0.065. This is around a 23% reduction in percent difference per 0.025 increase in Manning's n.

Thereafter, the slope is gentler with around an 8% rate of change per 0.025 increase in the Manning's n from 0.08 to 0.2. For the other three parameters shown, on average, the rate of reduction was smaller, ranging from 5% to 10% per every 0.025 increase in Manning's n. The exception was for the Manning's n ranging from 0.065 to 0.1, when the slope flattened.

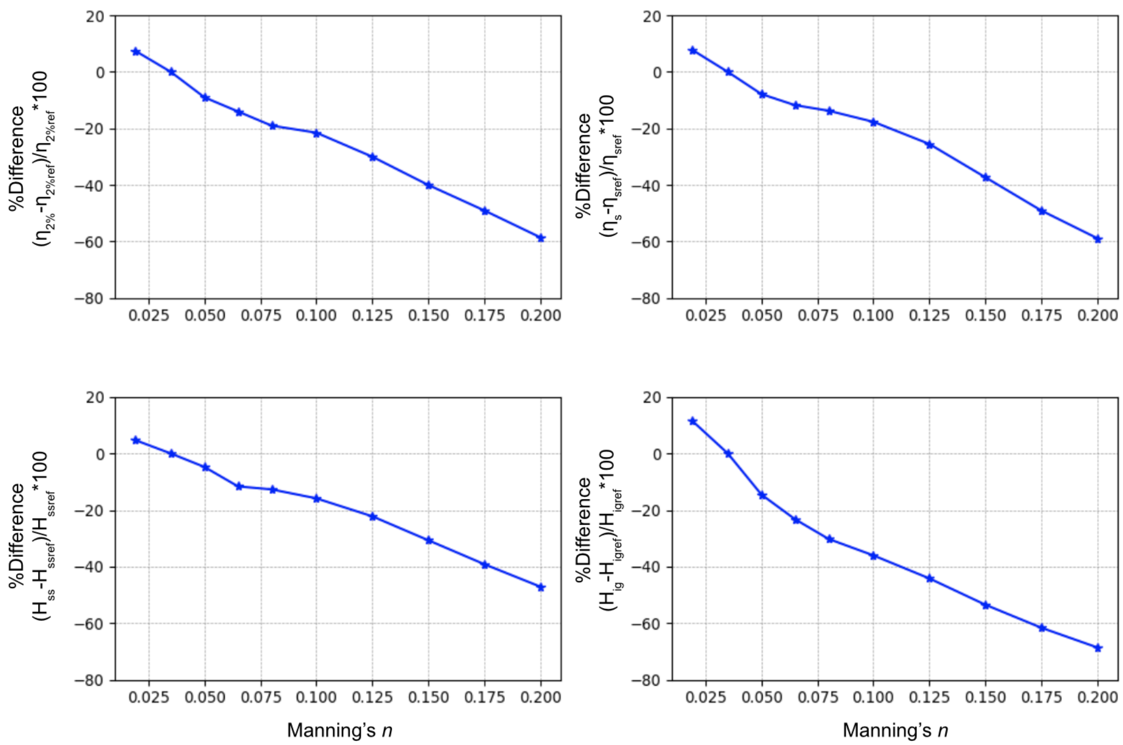

Figure 4.6: Percent differences between 10 test cases (that vary the Manning's n friction coefficient from 0.019 and 0.2) and the defined reference simulation (using Manning's n of 0.035) at a point along the 2 m isoline, near Rock Piles Beach, are shown for $\eta_{2\%}$ (top left), η_s (top right), H_{ss} (bottom left), and H_{ig} (bottom right).

4.7 Dimensionality

The most computationally feasible way to generate a forecast from SWASH is through a 1D modeling approach. This approach not only allows a forecast to be generated for a particular location in seconds to minutes, but it also enables forecasts to be produced for many locations along a particular coast. For these cases, simulations only contain one direction within a flume ($\partial x/\partial y = 0$). This indicates that the model solely considers the effects of waves along a transect and does not capture the interactions of waves over the reef in the along-shore direction.

For a more realistic representation of wave behavior in complex coastal environments where features such as headlands, bays, channels, and underlying spatial variabilities exist, a 2D modeling approach is suggested (*Torres-Freyermuth et al.*, 2012). This provides a more accurate depiction of how wave energy is transformed over the reef through wave interactions due to refraction, diffraction, and currents over the reef. In many scenarios, these interactions accounted for in a 2D configuration converge on solutions with higher wave heights than those predicted by a 1D model. This section highlights the magnitude of these differences between 1D and 2D simulations.

4.7.1 Model Sensitivity to Bottom Irregularities

Guiles et al. (2019) provided cases highlighting large spatial variabilities of wave energy simulated across the reef within the SS and IG bands along the west Maui Coast from a seasonal northerly swell event for Hawaii ($H_s = 2$ m and $T_p = 18$ seconds) using the BOSZ model. *Torres-Freyermuth et al.* (2012) noted that the non-uniformity of extreme water levels simulated by SWASH for a fringing reef lagoon suggests that two-dimensional effects must be incorporated and deserve further investigation. *Caldwell and Aucan* (2007) discussed large variabilities along the north shore of Oahu, where incoming energy becomes focused and amplifies breaking waves in the surf zone - and defined them as zones of maximum refraction due to non-uniform seafloor topography.

Figure 4.7 provides an example of how wave energy focuses in these zones of maximum refraction over the reef within the IG bands from a SWASH simulation using similar boundary conditions that *Guiles et al.* (2019) used. Although IG band heights, in general, increase in the cross-shore direction toward the beach as wave energy shifts from the higher sea and swell bands, a significant amount of along-shore variability is highlighted with IG band heights ranging from less than a meter to near 2 m due to the aforementioned coastal irregularities.

Additionally, different swell directions can lead to these hot spots of IG energy shifting to different locations along the coast, further emphasizing the necessity of 2D simulations over 1D simulations.

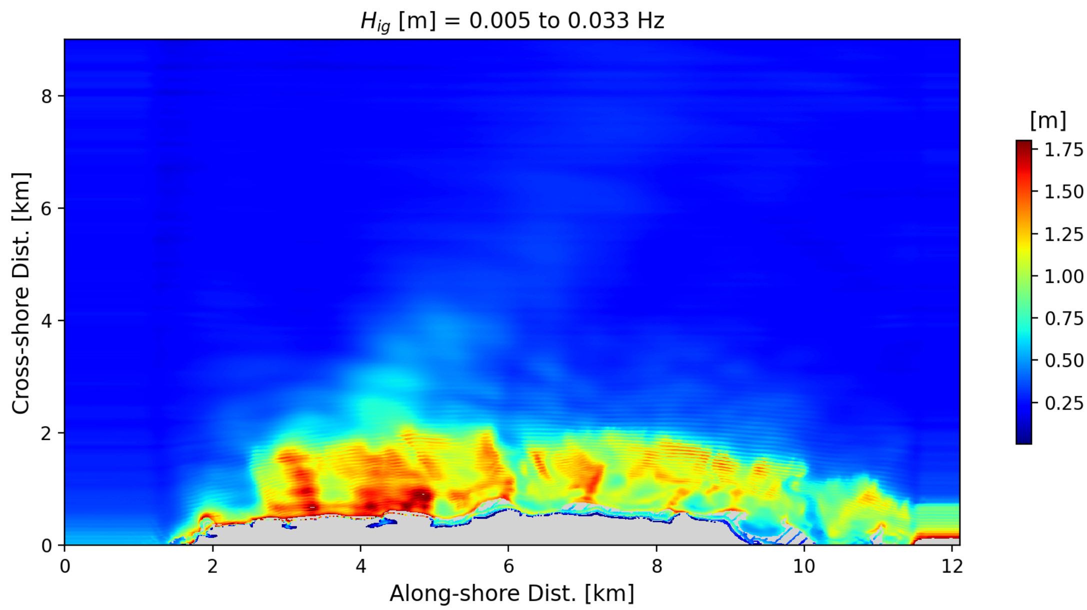

Figure 4.7: Simulated IG band height by SWASH, with $H_s = 2$ m and $T_p = 18$ seconds used for boundary conditions.

4.7.2 Wave Spectra: 2D vs. 1D

Figure 4.8 shows the computed spectra from four test simulations using $H_s = 2$ m and $T_p =$ 18 seconds to force the open grid boundary. Two simulations include water levels added over the reef reflecting a local high tide scenario for a 2D and 1D simulation. This is repeated in tests three and four, with water levels reflecting a local low tide scenario.

The most significant differences occur at the 2 m output point when the energy within the IG bands becomes the dominant portion of the spectrum after wave transformation. The 95% confidence intervals capture this and show a statistically significant spectral peak centered around the 0.01 frequency band. Table 4.6 highlights these differences at the 2 m output point and shows minimal influence from the change in water level but significant differences between the 2D and 1D simulations. IG band heights from the 2D results range from 55% to 68% of the 1D computations. Similar differences are shown within the SS bands, except the output from the 1D simulations ranges from 65% to 77% of the 2D. Provided a more accurate representation of the wave interactions over the reef yielded the 2D solutions, the conclusion is that 1D simulations overestimate the redistribution from the sea and swell to infragravity bands. Thus, any benefit gained in efficiency by utilizing 1D simulations may be offset by large (up to a factor of three) errors in low-frequency wave-driven water level variability, which may lead to poor operational guidance on inundation risk.

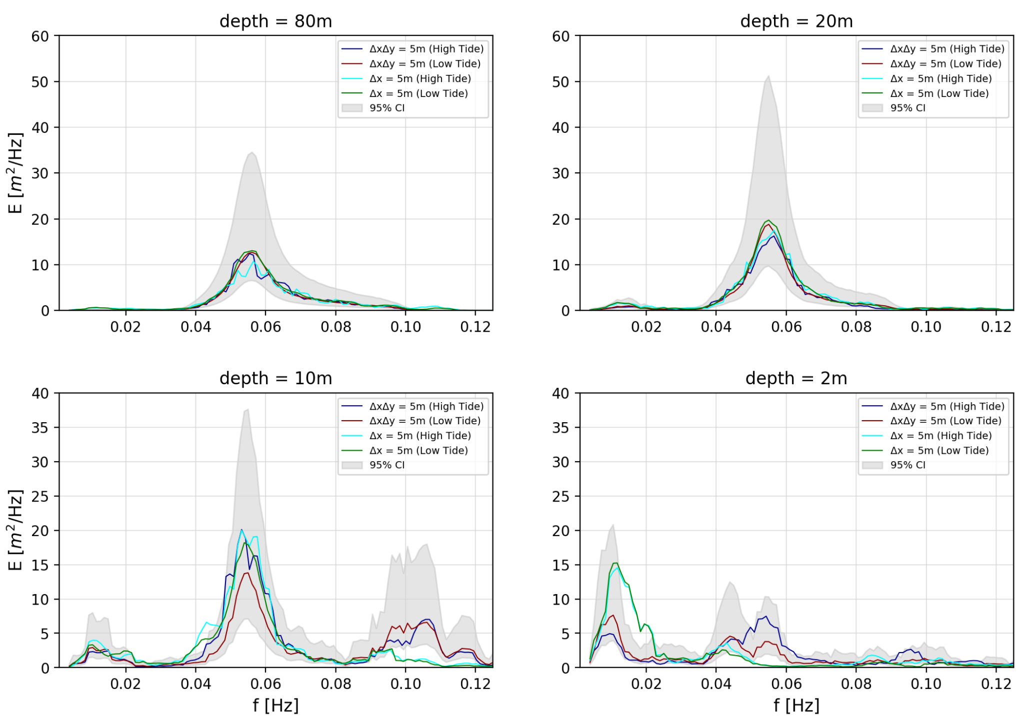

Figure 4.8: 2D (Δx, Δy) vs. 1D (Δx) 5 m (resolution) simulated wave spectra at locations along a transect from seaward of the reef at 80 m (top left) to the toe of the beach at 2 m (bottom right). Four test simulations using $H_s = 2$ m and $T_p = 18$ seconds as boundary conditions are shown, while varying the water levels reflecting local high and low tide scenarios. The 95% CI is only applied to the 2D test at low tide, for clarity.

Table 4.6: 2D vs. 1D differences (m) for high and low tide simulations.

Dimension	Grid Size	Depth	$\eta_{2\%}$	η_s	H_{ss}	H_{ig}
2D $\Delta x, \Delta y$ (High Tide)	5 m	2 m	1.61	0.32	1.77	0.93
1D (Δx) (High Tide)	5 m	2 m	1.40	0.04	1.35	1.64
2D $\Delta x, \Delta y$ (Low Tide)	5 m	2 m	1.28	0.11	1.71	1.07
1D (Δx) (Low Tide)	5 m	2 m	1.26	0.11	1.12	1.56

4.8 Efficiency vs. Computational Expense as a Function of Resolution

Phase-resolving models, such as SWASH, require a high spatial resolution, on the order of meters, to adequately capture the transformation of individual waves propagating from the deep water to the shore and their behavior in and around critical coastal features. This level of granularity, combined with the proposed 2D configuration discussed in section 4.7, poses enormous challenges for model implementation in an operational forecast environment. In general, the relationship between efficiency and computational expense as a function of spatial resolution is complex and nonlinear. At lower spatial resolutions, increasing the resolution can result in a more accurate solution with a small increase in computational costs. However, at higher spatial resolutions, the improvement in accuracy may be small compared to the increase in computational costs, leading to diminishing returns in efficiency. Therefore, an operational forecast office must balance the desired level of accuracy with the available computational resources and the practicality of running the model. Our aim is to determine the trade-off between efficiency and computational cost as a function of resolution in the absence of real-time observations.

4.8.1 CPU Architecture and Benchmark Platform

All tests are benchmarked on a single, multi-core Linux platform (Table 4.7) using the parallel version (MPI - Message Passing Interface) of SWASH, so the workload is distributed (using 48 of the available cores). The simulation time of each test (wall clock time; total real-world time elapsed) will be evaluated and compared against a reference simulation that will be discussed in the following section.

Table 4.7: Summary of System Configuration and CPU Information

Operating System	
Version	Ubuntu 20.04.3 LTS
CPU Information	
Model name	Intel(R) Xeon(R) Platinum 8168 CPU @ 2.70GHz
Architecture	x86_64
CPU op-mode(s)	32-bit, 64-bit
Byte Order	Little Endian
Address sizes	46 bits physical, 48 bits virtual
System Configuration	
CPU(s)	96
Thread(s) per core	2
Core(s) per socket	24
Socket(s)	2
Memory (total)	187 Gb
Swap	7 Gb

4.8.2 Results

Figure 4.9 quantifies how strongly the resolution can influence the model output along the 2 m contour for $\eta_{2\%}$ (top left), η_s (top right), H_{ss} (bottom left), and H_{ig} (bottom right), with percent differences between the tests and reference simulation (purple vertical line) decreasing as the resolution and computational expense increase. Each box plot reflects the distribution of solutions along the 2 m contour for spatial resolutions tested ranging from 5 m to 20 m. Provided the nonlinear behavior previously mentioned for computational expense involved, wall-clock time for each test is shown in exponential format along the X-axis, ranging from seconds for the 1m-1D simulation (gray box plot) to near 100 hours for the 3m-2D reference simulation.

Large negative biases are highlighted for resolutions between 12 m and 20 m, where percent differences dip into the -20 to -50 percent range. Note how the output from the coarse simulations (12 m, 15 m, and 20 m) begin to align or converge with the 1m-1D results shown in the gray box plot for $\eta_{2\%}$ and H_{ss}, which emphasizes the use of 2D configurations. The speed-accuracy trade-off on this computing platform is found between the 10 m and 8 m resolutions, where wall-clock times are held to three hours or less, and strong convergence is shown with percent differences dropping within the desired 10 percent margin of error range. Although optimal results are shown for the 5 m resolution output, a simulation time that triples (12 to 13 hour wall-clock time) the 8m test may not be feasible in an operational environment. This confirms that as resolution increases significantly, between 8m and 5m in this example, the improvement in accuracy becomes smaller with diminishing returns in terms of efficiency.

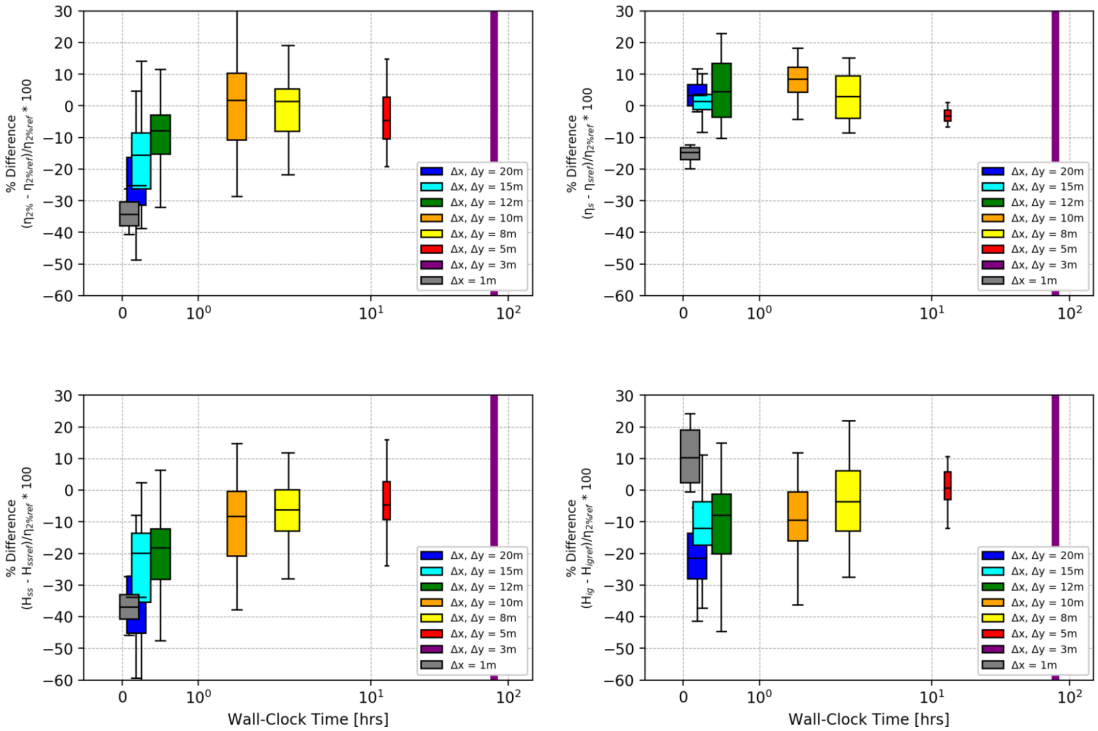

Figure 4.9: Box and whisker plots displaying the 2D SWASH output along the 2 m contour for resolutions ranging from 5 m to 20 m. Percent differences between the tests and the reference simulation are displayed as a function of wall-clock time along the X-axis. The gray box plot reflects the output from the 1m-1D simulation.

Chapter 5

Conclusions and Recommendations

The Pacific Islands pose significant challenges for implementing numerical models capable of accurately simulating wave transformations and wave-induced water levels in reef environments, particularly within operational forecast environments such as NOAA's NWS Forecast Offices across the Pacific, including Hawaii, Guam, and American Samoa. Their geographic location in the Pacific, combined with complex coasts characterized by a high degree of along-shore variability over the reef and steep reef slopes, make them uniquely different from the shores found elsewhere along the U.S. west and east coasts and in the Gulf of Mexico that most modeling platforms with the NWS are developed for.

Although many ongoing modeling efforts and support from the UH-ORE and PacIOOS use phase-resolving models operationally, such as BOSZ, none are currently implemented operationally within the NWS. This is a significant limitation in operations where forecasters frequently provide decision support services to core partners within Ocean Safety and the Emergency Management sectors regarding the potential for coastal inundation during extreme wave events each year.

Operational wave and water-level guidance made available to forecasters at the forecast offices include the NWPS that produces high-resolution wave guidance across the state and gridded composite storm surge risk maps associated with landfalling hurricanes for each island derived from the tightly coupled SLOSH-SWAN modeling system. Even though the NWPS accounts for water level input from the ESTOFS, it is a one-way coupled system, which means only the output of the phase-averaged wave heights from NWPS are influenced, but water levels input from ESTOFS remains unchanged by the waves through the forecast. Outside of empirically-derived guidance developed locally by *Caldwell et al.* (2009) that correlated coastal impacts with tide and surf predictions for only the north shore of Oahu, Hawaii, there is no numerical guidance for wave-driven water levels supporting forecast operations within the NWS modeling community for the Hawaiian Islands. The same issues exist for other NWS forecasters in the Pacific Region in American Samoa and Guam.

In this thesis, we presented an evaluation of the phase-resolving model SWASH on the north shore of Oahu, Hawaii, intending to determine the feasibility of running an on-demand 2D gridded model configuration in an operational forecast environment. The selection of SWASH was only practical, given its close relationship with SWAN, regarding the model setup and configuration, that is, the core wave model within the NWPS running operationally at the NWS. SWASH validation results have proven its applicability in a reef environment (*Zijlema*, 2012), where the significance of low-frequency wave energy that evolves and resonantly amplifies toward the shore through wave transformation after incipient breaking has a considerable impact on the observed water levels that can lead to inundation along reef-fronted coasts during extreme wave events.

This evaluation identified several controllable input variables that should be evaluated leading up to operational implementation. These variables were found to strongly influence the output from SWASH through a sensitivity analysis using idealized boundary conditions and water levels. These variables included simulation time, bottom friction, dimensionality, and computational cost as a function of resolution. Output parameters computed from the simulated surface elevations used to assess model performance were the two-percent exceedance wave height $\eta_{2\%}$, wave setup η_s, sea and swell height H_{ss}, and infragravity wave height (H_{ig}) along the 2m isoline and in the cross-shore direction along a transect to evaluate where the model sensitivity was greatest. Here is a summary of our conclusions:

Model simulation time: To assess SWASH simulation stability, crucial for reliable results, a model time convergence test is essential. Our 2D domain (12 km x 9 km) with low-frequency swell boundary conditions showed strong convergence within one to two-hour simulation times. Thus, a two-hour simulation time was deemed optimal for the model evaluation.

Friction: Provided its ability to capture surf zone dynamics more effectively, we employed the Manning formulation for all tests. The tests underscored heightened sensitivity to the Manning's n roughness factor near the shore, particularly along the 2 m isoline. Given this sensitivity and the spatial variability of coral coverage, considering variable friction factors could help address uncertainty and reduce potential biases.

Dimsensionality: While 1D modeling approaches provide computational efficiency and rapid forecast generation, they struggle to capture the important interactions of waves over reefs, especially in areas with significant bottom irregularities. These simulations represent wave solutions along a single transect, overlooking crucial along-shore interactions. Analysis revealed notable differences within the IG band solutions, which are significant contributions to water level forecasts, near the shore between 1D and 2D simulations. In contrast, 2D modeling approaches offer a more realistic depiction of wave behavior and transformations in complex coastal environments.

Efficiency vs. computational expense as a function of resolution: The relationship between efficiency and computational expense varies with spatial resolution nonlinearly. While increasing resolution can improve precision, it may lead to diminishing returns in efficiency at higher resolutions due to increased computational costs. Therefore, operational forecast offices must balance precision with available resources. The speed-accuracy trade-off on the computing platform used in this evaluation is found between the 10 m and 8 m resolutions, where wall-clock times are held to three hours or less, and strong convergence is shown with percent differences dropping within the desired 10 percent margin of error range.

An on-demand SWASH configuration is recommended for operational forecast offices due to the computational expense of 2D simulations. With an on-demand setup, forecasters can trigger simulations with a desired set of boundary conditions and water levels expected during the peak of an approaching event. Determining the critical areas for simulation can be based on various factors, including social information such as population density and previous experience with flooding from similar events. This approach benefits emergency planning by providing a worst-case estimate of potential coastal flooding in specific areas, helping authorities allocate resources and implement action plans more effectively.

As computational resources improve and additional optimizations are introduced in SWASH, operational forecast offices could explore running the model in production mode for 12 to 48 hours, aligning with the watch or warning phases defined by the NWS. In operational settings, forecasters typically require model results within a few hours to make more effective warning decisions. To meet these time constraints, wall-clock times for simulations could be reduced by leveraging the hot start functionality in SWASH. This feature allows users to initiate simulations from a previously saved steady state, eliminating the need for model spin-up periods and saving considerable computation time. Additionally, migrating from rectilinear to unstructured grids, with varying grid cell spacing from coarse seaward of the reef to fine near the coast, would enable larger domain sizes and expanded coastal coverage while maintaining model return times.

In summary, the implementation of SWASH would offer invaluable guidance to NWS forecasters at offices responsible for reef-lined coasts across the Pacific, effectively addressing the challenges of wave-driven inundation. SWASH is a powerful source of numerical guidance that can accurately predict various parameters required at operational forecast offices, including wave heights near the shore (shore break hazards) after transformation, wave-induced water levels, rip currents, wave runup, and inundation. The model can also be used to study the effects of sea level rise on wave transformation and predict the level of impacts associated with extreme events in vulnerable coastal areas that will be experienced in the future. The results could provide critical stakeholders with the necessary tools to make more effective coastal planning decisions to mitigate future risks.

Chapter 6

References

Aucan, J., R. Hoeke, and M. A. Merrifield (2012), Wave-driven sea level anomalies at the midway tide gauge as an index of north pacific storminess over the past 60 years, *Geophysical Research Letters*, *39*(17), L17,603, doi:10.1029/2012GL052993, hal-00798722.

Azouri, A. (2016), Observations, Forecast, and Modeling of 0.5-200 Min Infragravity Oscillations in Hale‘iwa Harbor Region, Hawai‘i, PhD dissertation, University of Hawaii, Honolulu, HI.

Bertin, X., et al. (2018), Infragravity waves: From driving mechanisms to impacts, *Earth-Science Reviews*, *177*, 774–799, doi:10.1016/j.earscirev.2018.01.002.

Booij, N., R. C. Ris, and L. H. Holthuijsen (1999), A third-generation wave model for coastal regions 1. model description and validation, *Journal of Geophysical Research: Oceans*, *104*, 7649–7666, doi:10.1029/98JC02622.

Caldwell, P. (2005), Validity of north shore, oahu, hawaii surf observations, *Journal of Coastal Research*, *21*(6), 1127–1138.

Caldwell, P. C., and J. P. Aucan (2007), An empirical method for estimating surf heights from deepwater significant wave heights and peak periods in coastal zones with narrow shelves, steep bottom slopes, and high refraction, *Journal of Coastal Research*, *23*, 1237–1244, doi:10.2112/04-0397R.1.

Caldwell, P. C., et al. (2009), Frequency and duration of coinciding high surf and tides along the north shore of oahu, hawaii, 1981-2007, *Journal of Coastal Research*, *25*(3), 734–743.

Chawla, A., H. L. Tolman, V. Gerald, D. Spindler, T. Spindler, J. H. G. Alves, D. Cao, J. L. Hanson, and E. M. Devaliere (2013), A multigrid wave forecasting model: A new paradigm in operational wave forecasting, *Weather and Forecasting*, *28*, 1057–1078, doi:10.1175/WAF-D-12-00007.1.

Cialone, M., and J. Smith (2007), Wave transformation modeling with bottom friction applied to southern Oahu reefs, *10th International Workshop on Wave Hindcasting and Forecasting Coastal Hazard Assessment*.

Filipot, J.-F., and K. F. Cheung (2012), Spectral wave modeling in fringing reef environments, *Coastal Engineering*, *67*, 67–79, doi: https://doi.org/10.1016/j.coastaleng.2012.04.005.

Fletcher, C. H., et al. (2008), Geology of hawaii reefs, *Coral Reefs of the USA*, pp. 435–487, doi:10.1007/978-1-4020-6847-8_11.

Franklin, E. C., P. L. Jokiel, and M. J. Donahue (2013), Predictive modeling of coral distribution and abundance in the hawaiian islands, *Marine Ecology Progress Series*, *481*, 121–132, doi:10.3354/meps10252.

Funakoshi, Y., J. Feyen, F. Aikman, H. Tolman, A. V. der Westhuysen, A. Chawla, I. Rivin, and A. Taylor (2012), Development of extratropical surge and tide operational forecast system (estofs), pp. 201–212, American Society of Civil Engineers, doi: 10.1061/9780784412411.00012.

Gerritson, F. (1981), Wave attenuation and wave set-up on a coastal reef., *in: Proc. Seventeenth Coastal Engng. Conf., (Sydney, Australia: Mar.23-28, 1980)*, *1* , *New Yo*, 444–461, doi:10.9753/icce.v17.27.

Guiles, M., A. Azouri, V. Roeber, M. M. Iwamoto, F. Langenberger, and D. S. Luther (2019), Forecasts of wave-induced coastal hazards in the united states pacific islands: Past, present, and the future, *Frontiers in Marine Science*, *6*, doi:10.3389/fmars.2019.00170.

Jelesnianski, C., J. Chen, and W. Shaffer (1992), Slosh: Sea, lake, and overland surges from hurricanes, *NOAA Technical Report NWS 48*, National Oceanic and Atmospheric Administration, U.S. Department of Commerce.

Longuet-Higgins, M. S., and R. W. Stewart (1962), Radiation stress and mass transport in gravity waves, with application to 'surf beats', *Journal of Fluid Mechanics*, *13*, 481–504, doi:10.1017/S0022112062000877.

Lowe, R. J., J. L. Falter, M. D. Bandet, G. Pawlak, M. J. Atkinson, S. G. Monismith, and J. R. Koseff (2005), Spectral wave dissipation over a barrier reef, *Journal of Geophysical Research: Oceans*, *110*, 1–16, doi:10.1029/2004JC002711.

Luettich, R., J. Westerink, and N. Scheffner (1992), Adcirc: An advanced three-dimensional circulation model of shelves, coasts, and estuaries, report 1: Theory and methodology of adcirc-2ddi and adcirc-3dl, *Technical Report DRP92-6*, U.S. Department of the Army.

Lynett, P. J. (2006), Wave breaking velocity effects in depth-integrated models, *Coastal Engineering*, *53*(4), 325–333, doi:https://doi.org/10.1016/j.coastaleng.2005.10.020.

Manning, R. (1891), On the flow of water in open channels and pipes, *Transactions of the Institution of Civil Engineers of Ireland*, *20*, 161–207.

Massel, S. R., and M. R. Gourlay (2000), On the modelling of wave breaking and set-up on coral reefs, *Coastal Engineering*, *39*, 1–27, doi:10.1016/S0378-3839(99)00052-6.

Mehra, A., and I. Rivin (2010), A real time ocean forecast system for the north atlantic ocean, *Terrestrial, Atmospheric and Oceanic Sciences*, *21*, 211, doi: 10.3319/TAO.2009.04.16.01(IWNOP).

Merrifield, M. A., J. M. Becker, M. Ford, and Y. Yao (2014), Observations and estimates of wave-driven water level extremes at the marshall islands, *Geophysical Research Letters*, *41*, 7245–7253, doi:10.1002/2014GL061005.

Munk, W. H. (1949), Surf beats, *Eos, Transactions American Geophysical Union*, *30*, 849–854, doi:10.1029/TR030i006p00849.

NGDC (2011), Oahu, hawaii 1/3 arc-second mhw coastal digital elevation model, https://www.ncei.noaa.gov/access/metadata/landing-page/bin/iso?id=gov.noaa.ngdc.mgg.dem:3410.

Pearson, S. G., C. D. Storlazzi, A. R. van Dongeren, M. F. S. Tissier, and A. J. H. M. Reniers (2017), A bayesian-based system to assess wave-driven flooding hazards on coral reef-lined coasts, *Journal of Geophysical Research. Oceans*, *122*(12), 10,099–117, doi: 10.1002/2017JC013204.

Roeber, V., and K. F. Cheung (2012), Boussinesq-type model for energetic breaking waves in fringing reef environments, *Coastal Engineering*, *70*, 1–20, doi: 10.1016/j.coastaleng.2012.06.001.

Roeber, V., J. Pinault, D. Morichon, S. Abadie, A. Azouri, M. Guiles, D. Luther, M. Delpey, and N. Danglade (2019), Improving wave run-up forecasts – benefits from phase-resolving models, in *Coastal Structures 2019*, edited by N. Goseberg and T. Schlurmann, pp. 752–761, Bundesanstalt für Wasserbau, Karlsruhe, doi:10.18451/978-3-939230-64-9.075.

Roelvink, Reniers, V. Dongeren, de Vries, McCall, and Lescinski (2009), Modelling storm impacts on beaches, dunes and barrier islands, *Coastal Engineering*, *56*, 1133–1152.

Sheremet, A., J. M. Kaihatu, S. F. Su, E. R. Smith, and J. M. Smith (2011), Modeling of nonlinear wave propagation over fringing reefs, *Coastal Engineering*, *58*, 1125–1137, doi:10.1016/j.coastaleng.2011.06.007.

Shi, F., J. T. Kirby, J. C. Harris, J. D. Geiman, and A. R. Grilli (2012), A high-order adaptive time-stepping tvd solver for boussinesq modeling of breaking waves and coastal inundation, *Ocean Modelling*, *43*, 36–51.

Smit, P., M. Zijlema, and G. Stelling (2013), Depth-induced wave breaking in a non-hydrostatic, near-shore wave model, *Coastal Engineering*, *76*, 1–16, doi: 10.1016/j.coastaleng.2013.01.008.

Smith, J. M., J. J. Westerink, A. B. Kennedy, A. A. Taflanidis, K. F. Cheung, and T. D. Smith (2011), Swims hawaii hurricane wave, surge, and runup inundation fast forecasting tool, pp. 89–98, American Society of Civil Engineers, doi:10.1061/41185(417)9.

Stockdon, H. F., R. A. Holman, P. A. Howd, and A. H. Sallenger (2006), Empirical parameterization of setup, swash, and runup, *Coastal Engineering*, *53*, 573–588, doi:10.1016/j.coastaleng.2005.12.005.

The SWASH Team (2023), *SWASH – Implementation Manual. Delft University of Technology, Environmental Fluid Mechanics Section*, version 10.01.

Tissier, M., P. Bonneton, F. Marche, F. Chazel, and D. Lannes (2012), A new approach to handle wave breaking in fully non-linear boussinesq models, *Coastal Engineering*, *67*, 54–66, doi:https://doi.org/10.1016/j.coastaleng.2012.04.004.

Tognacchini, C. (2023), Wave Energy Tranformations in a Complex Environment; Observations, Modeling, and Applications, Master's thesis, University of Hawaii, Honolulu, HI.

Tolman, H. L., B. Balasubramaniyan, L. D. Burroughs, D. V. Chalikov, Y. Y. Chao, H. S. Chen, and V. M. Gerald (2002), Development and implementation of wind-generated ocean surface wave models at ncep, *Weather and Forecasting*, *17*, 311–333, doi:10.1175/1520-0434(2002)017¡0311:DAIOWG¿2.0.CO;2.

Torres-Freyermuth, A., I. Mariño-Tapia, C. Coronado, P. Salles, G. Medellín, A. Pedrozo-Acuña, R. Silva, J. Candela, and R. Iglesias-Prieto (2012), Wave-induced extreme water levels in the puerto morelos fringing reef lagoon, *Natural Hazards and Earth System Science*, *12*, 3765–3773, doi:10.5194/nhess-12-3765-2012.

Tucker, M. J. (1950), Surf beats: sea waves of 1 to 5 min. period, pp. 565–573, doi:10.1098/rspa.1950.0120.

Van der Westhuysen, A., D. Eversole, and J. Feyen (2011), Coastal Inundation Model Guidance for the Pacific Islands, [Online; 20th October 2011].

Van der Westhuysen, A. J., R. Padilla-Hernandez, P. Santos, A. Gibbs, D. Gaer, T. Nicolini, S. Tjaden, E. M. Devaliere, and H. L. Tolman (2013), Development and validation of the nearshore wave prediction system, in *Proc. 93rd AMS Annual Meeting*, American Meteorological Society, Austin.

Vetter, O., J. M. Becker, M. A. Merrifield, A. C. Pequignet, J. Aucan, S. J. Boc, and C. E. Pollock (2010), Wave setup over a pacific island fringing reef, *Journal of Geophysical Research: Oceans*, *115*, doi:10.1029/2010JC006455.

Walker, R. A. (2017), Short-term shoreline change on oahu's north shore during a strong el niño year, Master's thesis, University of Hawaii, submitted to the Graduate Division of the University of Hawaii in partial fulfillment of the requirements for the degree of Master of Geoscience, Department of Geology and Geophysics.

Zijlema, M. (2012), Modelling wave transformation across a fringing reef using swash. coast eng proc 1(33) (currents.26), doi:10.9753/icce.v33.currents.26.

Zijlema, M., G. Stelling, and P. Smit (2011), Swash: An operational public domain code for simulating wave fields and rapidly varied flows in coastal waters, *Coastal Engineering*, *58*, 992–1012, doi:10.1016/j.coastaleng.2011.05.015.